PHYSICAL REVIEW A **79**, 062708 (2009)

Low-energy collisions of NH_3 and ND_3 with ultracold Rb atoms

Piotr S. Żuchowski* and Jeremy M. Hutson†
Department of Chemistry, Durham University, South Road, Durham DH1 3LE, United Kingdom
(Received 26 February 2009; published 11 June 2009)

We carry out quantum inelastic scattering calculations of collisions of Rb atoms with inverting NH_3 and ND_3 molecules in the energy range between 0 and 100 cm^{-1}, which are important for experiments using velocity-controlled molecular beams to probe scattering resonances. We focus on molecules initially in the upper level of the ammonia inversion doublet for $j=1$, $k=1$, which is low-field seeking and can be controlled in a Stark decelerator. We calculate the integral elastic and state-to-state inelastic cross sections in the coupled-states approximation. We demonstrate the presence of both shape and Feshbach resonances in the elastic and inelastic cross sections at low collision energies and discuss their origin in terms of the bound states of the Rb-ND_3 complex. We also consider elastic and inelastic cross sections in the ultracold regime, using close-coupling calculations, in order to assess the viability of sympathetic cooling of ND_3 by Rb. The inelastic cross section for relaxation to the lower level of the inversion doublet is smaller than expected for such a strongly coupled system but is still likely to be too large to allow sympathetic cooling for ND_3 in low-field-seeking states. However, there is a good prospect that sympathetic cooling will be possible for molecules in high-field-seeking states even when the collision partner is a magnetically trapped atom in a low-field-seeking state.

DOI: 10.1103/PhysRevA.79.062708 PACS number(s): 34.50.Cx, 37.10.Mn, 34.20.−b

I. INTRODUCTION

Over the last few years, several methods have been developed to cool molecules to temperatures below 1 K. These include buffer-gas cooling in cryogenic helium [1,2], Stark deceleration with switched electric fields [3,4], velocity filtering [5], optical deceleration with laser fields [6], and crossed molecular beam scattering [7]. The availability of cold molecules opens up a new field of low-energy collision studies in a novel regime where collisions are dominated by long-range forces and resonances.

Stark decelerators can be used to *control* beam velocity as well as to reduce it [8]. Pulsed molecular beams can be generated with much smaller velocity spreads than is possible with conventional supersonic sources. This offers the opportunity to study scattering resonances at much higher resolution than has been possible in the past. Gilijamse *et al.* [9] carried out a proof-of-concept experiment in which a velocity-controlled beam of OH radicals collided with Xe atoms in a jet. In this case the energy resolution of the experiment was limited to 13 cm^{-1} by the velocity spread of the Xe atoms. However, experiments are under way to collide two velocity-controlled beams, which will provide much higher resolution.

An alternative approach is to collide a beam with a sample of trapped atoms or molecules that are already nearly at rest. Sawyer *et al.* [10] recently measured collision cross sections for He atoms and H_2 molecules in pulsed beams colliding with magnetically trapped OH radicals and achieved a resolution of 9 cm^{-1}. Experiments to investigate the collisions of a velocity-controlled beam of ND_3 with trapped ultracold Rb atoms are also under way and again should be able to provide much better velocity resolution.

Scattering resonances in molecular collisions have been studied for many years [11] and can be very important in chemical reactions [12,13]. In simple systems where only a few partial waves contribute, they may produce sharp structures in cross sections as a function of collision energy [14,15]. However, in more complicated systems with dense energy level patterns, the resonant structures may get lost in the background. It is therefore important to explore whether well-defined resonant structures are expected for collisions of molecules that can be velocity controlled (such as ND_3 and OH) and atoms that can be laser cooled (such as alkali metal atoms).

In this paper we study collisions of Rb atoms with ND_3 and NH_3 for collision energies between 0 and 100 cm^{-1}. We carry out quantum-mechanical calculations of integral elastic and state-to-state inelastic cross sections using the coupled-states or centrifugal-sudden (CS) approximation and observe numerous scattering resonances. To understand the nature of the scattering processes, we study the resonance structure of the scattering cross sections for individual partial waves. The resonances can be explained in terms of the bound states of the Rb-ND_3 complex. We calculate the pattern of bound states near the lowest dissociation limits of the complex as a function of the end-over-end angular momentum and identify the bound states responsible for the resonances.

There is a further reason for being interested in Rb-NH_3 collisions. Methods such as Stark deceleration can slow molecules to velocities of a few meters per second, and the resulting molecules can then be trapped at temperatures of 10–100 mK [16,17]. It has not yet proved possible to cool such molecules further toward the temperatures and phase-space densities at which they might undergo condensation to form quantum gases. There is great interest in methods that might be used to achieve this, and one of the most promising is *sympathetic cooling* [18,19], in which molecules are cooled by thermal contact with a laser-cooled gas of atoms such as Rb. However, sympathetic cooling can work only if the collisions are predominantly elastic rather than inelastic: if the

*piotr.zuchowski@durham.ac.uk
†j.m.hutson@durham.ac.uk

molecules are in excited states and undergo inelastic (de-excitation) collisions, the kinetic energy released is usually enough to eject both collision partners from the trap. We therefore also carry out calculations of elastic and inelastic cross sections at the temperatures relevant to sympathetic cooling.

II. THEORY

A. Rb-NH_3 interaction potential

In previous work we obtained the potential energy surface for NH_3 interacting with Rb from highly correlated electronic structure calculations [20]. Spin-restricted coupled-cluster calculations including single, double, and perturbative triple excitations [RCCSD(T)] were carried out on a grid of points in the intermolecular distance R and intermolecular angles θ and χ. The angle χ corresponds to rotation of NH_3 about its C_3 axis. The angles θ_i were chosen to be the points for 20-point Gauss-Lobatto quadrature, which include $\theta=0°$ and 180° (with $\theta=0°$ corresponding to approach toward the lone pair of NH_3). Calculations were carried out on a grid of R values from $3.5a_0$ to $25a_0$ and for two azimuthal angles $\chi=0°$ and 60°.

For collision calculations, we need to evaluate matrix elements of the interaction potential between angular momentum basis functions. This is most easily achieved by expanding the potential in renormalized spherical harmonics $C_{\lambda\mu}(\theta,\chi)$. After taking account of the C_{3v} symmetry of NH_3, the expansion takes the form

$$V(R,\theta,\chi) = \sum_{\lambda=0,1,\ldots} \sum_{\mu=0,3,6,\ldots} \frac{1}{1+\delta_{\mu,0}} v_{\lambda\mu}(R) \times [C_{\lambda\mu}(\theta,\chi) + (-1)^{\mu} C_{\lambda,-\mu}(\theta,\chi)]. \quad (1)$$

The dominant terms in this expansion are those with $\mu=0$ and 3, and the corresponding coefficients may be written as

$$v_{\lambda\mu}(R) = \frac{\left(\lambda+\frac{1}{2}\right)}{2-\delta_{\mu 0}} \sqrt{\frac{(\lambda-\mu)!}{(\lambda+\mu)!}} \int P_{\lambda\mu}(\cos\theta) V_{\mu}(R,\theta) d\cos\theta, \quad (2)$$

where $P_{\lambda\mu}(\cos\theta)$ is an associated Legendre polynomial and

$$V_0(R,\theta) = \tfrac{1}{2}[V(R,\theta,0°) + V(R,\theta,60°)],$$

$$V_3(R,\theta) = \tfrac{1}{2}[V(R,\theta,0°) - V(R,\theta,60°)]. \quad (3)$$

V_0 can be viewed as the interaction potential averaged over χ, while V_3 describes the leading anisotropy of the potential with respect to rotation about the C_3 axis of NH_3. To obtain the expansion coefficients in Eq. (2) at a given value of R for Rb-NH_3, the potential functions $V_{\mu}(R,\theta_i)$ at each grid point θ_i are first evaluated by reproducing kernel Hilbert space (RKHS) interpolation [21,22] and the angular integrations are then carried out by Gauss-Lobatto quadrature.

For calculations on Rb-ND_3 we need to re-expand the potential in a coordinate system based on the center of mass of ND_3 instead of NH_3. This is done by first generating a set of points for Rb-ND_3 at the same grid of distances and angles as for Rb-NH_3. The center of mass of ND_3 is shifted by a distance δ toward the D atoms from that of NH_3. Each point is obtained by

$$V_{\text{Rb-ND}_3}(R,\theta,\chi) = V(R',\theta',\chi), \quad (4)$$

where

$$R' = R(1+t^2+2t\cos\theta)^{1/2},$$

$$\cos\theta' = (\cos\theta + t)R/R', \quad (5)$$

and $t=\delta/R$. The potential coefficients for Rb-ND_3 are then obtained by quadrature exactly as those for Rb-NH_3, but with the transformed set of points.

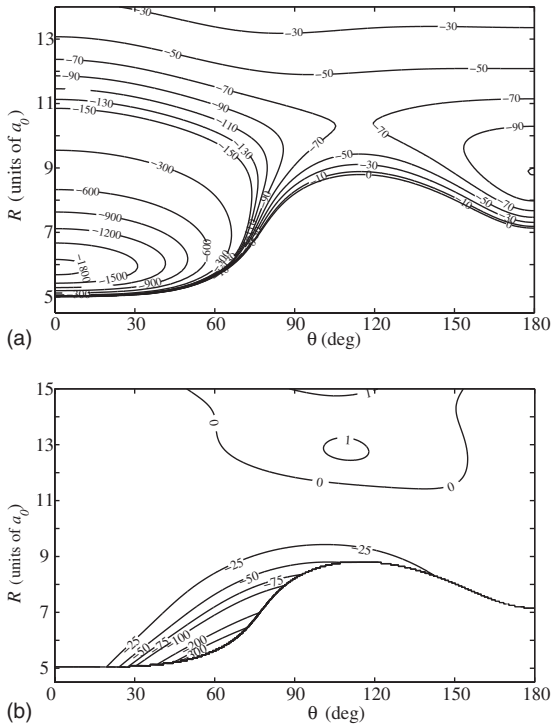

FIG. 1. The interaction potential of Rb-NH_3 from CCSD(T) calculations: $V_0(R,\theta)$ component (upper panel) and $V_3(R,\theta)$ component (lower panel). Contours are labeled in cm^{-1}. To aid visualization, V_3 is plotted only in the energetically accessible region defined by $V_0<0$.

The V_0 and V_3 interaction potentials for Rb-NH_3 are shown in Fig. 1. The potential is strongly anisotropic; there is a very deep minimum, nearly 1900 cm^{-1} deep, at the N side of NH_3. This is due to the interaction of the lone pair of NH_3 with the singly occupied $5s$ orbital of the Rb atom. There is also a shallow secondary minimum, only about 100 cm^{-1} deep, on the H side of NH_3, arising from dispersion interactions. Both minima are on the C_3 axis of NH_3. A detailed discussion of the alkali-atom–NH_3 interaction can be found in Ref. [20].

The basis set which we used in our previous work (augmented triple zeta for N and H and a basis set of triple-zeta quality for Rb) gave depths for the minima at linear geometries of 1862 and 110 cm^{-1} (for N-side and H-side configu-

rations, respectively). To improve this in the present work, we performed additional calculations for linear geometries near the minima with a significantly larger basis set. With the basis set extended to augmented quadruple zeta for N and H and with additional h functions on the Rb atom (with exponents 0.45 and 0.167) and an additional midbond g function (with exponent 0.4), we obtained a global minimum well depth of 1881 cm^{-1} with negligible (less than 0.1%) change in the equilibrium distance. All the potential points were then scaled by the ratio of the well depths calculated with quadruple-zeta and triple-zeta basis sets. The depth of the secondary minimum on the surface obtained by such scaling is 111 cm^{-1}, which agrees well with the value obtained from *ab initio* calculations with the quadruple-zeta basis set. In the scattering calculations described below we have used the scaled triple-zeta potential.

For very large Rb-NH_3 separations the expanded potential is dominated by the $v_{0,0}$ and $v_{2,0}$ terms, which vanish as R^{-6}. Since the inherent error of the supermolecular approach is quite significant at large R, we represent the long-range behavior of $v_{0,0}$ and $v_{2,0}$ using $C_{6,0}$ and $C_{6,2}$ coefficients obtained from perturbation theory [20]. At short range we switch over to the full expansion using a switching function $(1+\exp[a(R-b)])^{-1}$ with $a=0.5a_0^{-1}$ and $b=26a_0$.

B. Scattering calculations

The Hamiltonian that describes collisions between an atom and a molecule may be written as

$$\frac{\hbar^2}{2\mu}\left[-R^{-1}\frac{d^2}{dR^2}R+\frac{\hat{L}^2}{R^2}\right]+H_{\rm at}+H_{\rm mol}+V_{\rm inter}, \tag{6}$$

where μ is the reduced mass for the colliding pair, $\hat{L}^2$ is the operator for rotation of the collision partners about one another, and $H_{\rm at}$ and $H_{\rm mol}$ are the Hamiltonians for the isolated atom and molecule, respectively. In the special case where either the atom or the molecule is in a closed-shell singlet state, the main part of the interaction potential $V_{\rm inter}$ is a single potential energy surface $V(R,\theta,\chi)$ that couples the molecular rotations strongly to the intermolecular distance. The molecular rotations are in turn coupled to the nuclear spins in the molecule by hyperfine terms. However, for an atom in an S state the only terms that couple the molecular degrees of freedom to the *atomic* electron and nuclear spins are (i) very weak magnetic dipole-dipole interactions between atomic and molecular spins and (ii) any dependence of the atomic hyperfine coupling on the intermolecular distance R. If these very small terms are neglected, the collision problem may be treated as the scattering of the molecule from an *unstructured* atom.

The Hamiltonian of a rigid symmetric-top molecule may be written as

$$H_{\rm mol}=B\hat{j}^2+(C-B)\hat{j}_z^2, \tag{7}$$

where $\hat{j}^2$ is the operator representing the angular momentum of the molecule and $\hat{j}_z$ denotes its projection onto the molecule-fixed symmetry axis z, while C and B are the rotational constants for rotation about the symmetry axis and an axis perpendicular to it. The eigenfunctions of this Hamiltonian are labeled by three quantum numbers: j—the total angular momentum of the rotor, m—the projection of j on the laboratory-frame Z axis, and k—the projection of j on the body-fixed molecular symmetry axis z,

$$\hat{j}^2|jkm\rangle=j(j+1)|jkm\rangle,$$

$$\hat{j}_Z|jkm\rangle=m|jkm\rangle,$$

$$\hat{j}_z|jkm\rangle=k|jkm\rangle. \tag{8}$$

The N-H stretching vibrations are at sufficiently high frequency that they can be neglected in the present work, but NH_3 also has a bending (umbrella) vibration with two minima that are equivalent in the free molecule. Tunneling between these two minima produces a low-frequency splitting that corresponds to inversion of the molecule through a planar geometry. To describe this we introduce an additional degree of freedom, the inversion coordinate h. The vibration-inversion functions $|+\rangle$ and $|-\rangle$ (corresponding to the lower and upper components of the inversion doublet) may be written as

$$|\pm\rangle\sim[f(h_{\rm eq}-h)\pm f(h_{\rm eq}+h)], \tag{9}$$

where $f(x)$ is a function that is sharply peaked around $x=0$, so that $f(h_{\rm eq}\pm h)$ is a bending function that is sharply peaked around one of the equilibrium values $\mp h_{\rm eq}$ (corresponding to one of the individual "umbrella" states of NH_3).

NH_3 occurs in two different nuclear spin configurations, corresponding to A_1 and E symmetries. In the first case (referred to as ortho-NH_3) the molecule can occupy rotational levels with $k=0,3,6,\ldots$, while in the latter (referred to as para-NH_3) only $k=1,2,4,5\ldots$ are allowed. For ortho-NH_3 in $k=0$ states, only one component of each inversion doublet is allowed by symmetry. ND_3 is slightly different and occurs in three nuclear spin symmetries, A_1, A_2, and E. Molecules in nuclear spin states of A_1 and A_2 symmetries can occupy rotational levels with $k=0,3,6,\ldots$, referred to as ortho-ND_3, while those in the E state can occupy levels with $k=1,2,4,5,\ldots$, referred to as para-ND_3. Ortho- and para-species do not readily interconvert in collisions. By contrast with NH_3, however, ND_3 molecules in $k=0$ states can exist in both upper and lower components of the inversion doublet.

The rotational functions adapted for permutation-inversion symmetry may be written as [23]

$$[|jkm\rangle\mp(-1)^j|j-km\rangle]|\pm\rangle \tag{10}$$

for para-NH_3 and

$$[|jkm\rangle\pm(-1)^j|j-km\rangle]|\pm\rangle \tag{11}$$

for para-ND_3. If $f(h_{\rm eq}-h)$ and $f(h_{\rm eq}+h)$ do not overlap significantly, evaluation of the matrix elements of the potential between the symmetry-adapted basis functions gives expressions that are isomorphic to those for the case of a rigid symmetric top with parity-adapted monomer basis functions. It is therefore sufficient to carry out the scattering calculation exactly as for a rigid symmetric top but with the monomer

TABLE I. Rotational constants [29,30] and inversion splitting parameters (with centrifugal distortions) [28] used for NH_3 and ND_3. Units are cm^{-1}.

Parameter	NH_3	ND_3
B	9.9441	5.1428
C	6.2294	3.1142
ν_0	0.7934	5.337×10^{-2}
ν_a	5.05×10^{-3}	2.39×10^{-4}
ν_b	1.998×10^{-3}	9.61×10^{-5}

energies for the even and odd combinations of $|jkm\rangle$ and $|j-km\rangle$ shifted up and down from the rigid-rotor values by half the inversion splitting.

The approach of restricting the basis set of inversion functions to just the lowest pair of states was introduced by Green [23,24] and Davis and Boggs [25], but it was later verified to be a good approximation by Van der Avoird and co-workers [26,27], who carried out calculations on Ar-NH_3 collisions to compare with theory that took the h coordinate into account explicitly.

The rotational constants and inversion parameters used for NH_3 and ND_3 in the present paper are given in Table I. Since inelastic transitions between inversion states are of key interest for the present work, we allow the inversion splitting to be a function of rotational state [28],

$$\nu = \nu_0 - \nu_a[j(j+1) - k^2] - \nu_b k^2. \tag{12}$$

The energy levels for $j=1-3$ for both ortho- and para-NH_3 and ND_3 are given in Table II. In each case the zero of energy is the energy of the lowest allowed tunneling component for $j=0$, $k=0$.

In the following sections we identify tunneling components by u (upper) or l (lower) instead of symmetry labels because the u/l designation indicates the energetics more directly.

The Rb-NH_3 potential is very strongly anisotropic. Because of this, scattering calculations require large basis sets of rotational functions for convergence. In addition, we typically need to carry out calculations for many different total angular momenta (partial waves) to obtain all the contributions to integral cross sections. We typically need to include 100–200 partial waves at collision energies around 100 cm^{-1}.

The most accurate approach for quantum inelastic scattering is to use close-coupling calculations, which expand the total wave function for the collision system in a space-fixed basis set using a total angular momentum representation. In the present case the basis functions are labeled by quantum numbers $j,k,\pm$, which describe the monomer, and L, which describes the angular momentum for rotation of the collision partners about one another. For each total angular momentum J and total parity, full close-coupling (CC) calculations include all possible values of L allowed by angular momentum coupling for each monomer level $(j,k,\pm)$. However, such calculations give enormous basis sets for large J and are prohibitively expensive except at the very lowest energies (where only a few J values contribute to cross sections).

TABLE II. The energy levels of NH_3 and ND_3 molecules (up to $j=3$) used in the present calculations. Units are cm^{-1}. The labels o and p refer to ortho- and para-spin isomers. For NH_3 in $k=0$ states, only the $|(-1)^{j+1}\rangle$ inversion state is allowed for each j.

State	Spin isomers	NH_3	$\|\pm\rangle$	ND_3	$\|\pm\rangle$
00	o	0.0000	−	0.0000	+
00	o			0.0534	−
11	p	15.3871	+	8.2570	+
11	p	16.1735	−	8.3100	−
10	o	19.1049	+	10.2851	+
10	o			10.3385	−
22	p	44.0305	+	22.7424	+
22	p	44.8058	−	22.7949	−
21	p	55.1837	+	28.8282	+
21	p	55.9499	−	28.8802	−
20	o	59.6646	−	30.8568	+
20	o			30.9102	−
33	o	85.1365	+	43.4562	+
33	o	85.8969	−	43.5080	−
32	p	114.8786	+	59.6850	+
32	p	115.6145	−	59.7356	−
31	p	103.7254	+	53.5992	+
31	p	104.4704	−	53.6503	−
30	o	118.5964	+	61.7107	+
30	o			61.7641	−

A more affordable approach that is adequate at higher energies is provided by the CS approximation [31,32], which was introduced for atom-symmetric-top systems by Green [24]. In the CS approach the scattering equations are written in a body-fixed frame and for each partial wave the basis functions are labeled by the monomer quantum numbers $(j,k,\pm)$ and the projection K (helicity) of j onto the body-fixed intermolecular axis R. If the centrifugal operator is approximated by $L(L+1)/(2\mu r^2)$, with $L=J$ for all channels, then the coupled equations factorize into independent sets labeled by L and K. The size of the resulting basis sets is independent of L, so that the total cost of a scattering calculation scales linearly with the number of partial waves included. The CS approximation is generally expected to be accurate when the kinetic energy and the potential anisotropy are both large compared to the rotational constant of the collision complex.

C. Details of scattering calculations

We carry out coupled-channel scattering calculations using the MOLSCAT package [33] with the hybrid log-derivative–Airy propagator of Alexander and Manolopoulos [34]. The inner starting point for the integration was chosen to be $R=4.2a_0$, which is deep in the inner classically forbidden region. Since the potential for $\theta\approx0°$ is very deep, the

TABLE III. The convergence of typical cross sections (in Å^2) for Rb-ND_3 with respect to the maximum quantum numbers (j_{max},k_{max}) in the rotational basis set. The cross sections were calculated with the coupled-states method at an energy of 25 cm^{-1} with respect to $j=0$, $k=0$ level. The computer time taken for a single partial wave, relative to the time for the (21,8) basis set, is also given.

Basis	$\sigma_{11u\to11u}$	$\sigma_{11u\to11l}$	$\sigma_{22u\to11u}$	Time
(15,5)	1309	62.22	5.14	0.2
(18,5)	1292	59.42	3.89	0.3
(21,5)	1283	62.67	5.59	0.5
(15,8)	1296	57.39	4.94	0.3
(18,8)	1291	63.11	7.45	0.6
(21,8)	1293	59.70	3.90	1.0
(15,11)	1302	61.83	4.92	0.5
(18,11)	1291	62.09	5.77	0.9
(21,11)	1292	59.42	3.89	1.7

wave function oscillates very rapidly at short range. Thus in the inner region ($R<13a_0$) we use the fixed-interval log-derivative propagator [35] with a small step size of $0.015a_0$. The log-derivative matrix is then propagated from $13a_0$ to $400a_0$ with the variable-step Airy propagator, which takes very long steps at long range and consumes only a small part of the total computer time. The Airy propagator was used with convergence criterion TOLHI=10^{-4} [36]. The resulting inelastic and elastic cross sections are converged with respect to all integration parameters to better than 1%.

As mentioned above, the strong anisotropy of the potential energy surface causes slow convergence with respect to the basis set of monomer rotational functions, especially for ND_3, which has rotational constants about a factor of 2 smaller than NH_3. In Table III we show the convergence of selected integral cross sections for Rb-ND_3 together with relative computer times. The rotational basis set with $j_{max}=21$ and $k_{max}=8$, containing 210 monomer energy levels for para-ND_3, gives a good compromise between accuracy and computational cost: typical calculations for a single energy and K value take ~30 s on a 2.0 GHz single-core Opteron processor, which means that calculations of cross sections converged with respect to the partial-wave expansion take approximately 2 h per energy. For Rb-NH_3, a slightly smaller basis set with $j_{max}=14$ and $k_{max}=7$ gave cross sections converged to ~1%. All calculations are for ^{87}Rb.

III. RESULTS

A. Scattering cross sections

The ND_3 and NH_3 molecules can be slowed by Stark deceleration in their low-field-seeking $j=1$, $k=1$ states, which correlate at low field with the upper level of the inversion doublet. Since ND_3 has a much smaller tunneling splitting than NH_3, its Stark effect is more nearly linear and it is easier to decelerate. We have calculated the energy dependence of the state-to-state integral cross sections for molecules initially in the upper inversion state of ND_3 and NH_3 for collision energies between 0 and 100 cm^{-1}. The results are shown in Fig. 2.

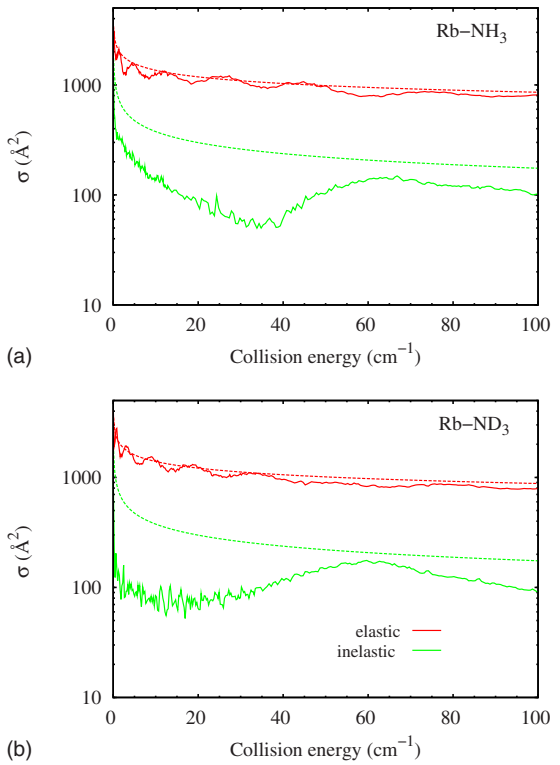

FIG. 2. (Color online) Elastic and total inelastic cross sections for Rb-NH_3 (upper panel) and Rb-ND_3 (lower panel) scattering from the upper component of the inversion doublet for the $j=1$, $k=1$ state. The smooth dashed lines show the results of the semiclassical background formula for elastic cross sections and of Langevin capture theory for the total inelastic cross sections.

For the whole energy range considered, the elastic cross sections $\sigma_{11u\to11u}$ are large compared to the total inelastic cross sections for both ND_3 and NH_3. Figure 2 includes the elastic cross section obtained from the semiclassical background formula [37] for a pure R^{-6} potential (dashed red line). For both Rb-NH_3 and Rb-ND_3 the elastic cross sections follow the background formula fairly closely, with slow glory oscillations superimposed on the background. The total cross sections (elastic+inelastic) are actually in even better agreement with the semiclassical model than the elastic cross sections. There is also structure due to scattering resonances at low collision energies, but it is not very strong with respect to the background for the elastic cross sections. At higher collision energies the resonances are lost in the background.

The overall magnitude of the inelastic cross sections is at first sight less than expected. In a strongly coupled system where every collision that crosses the centrifugal barrier leads to inelasticity, the total inelastic cross section is given by the Langevin capture formula [38],

$$k_{\text{capture}}^{\text{inel}} = 3\pi\left(\frac{C_6}{4E}\right)^{1/3}. \tag{13}$$

The Langevin result is shown as a dashed green line in Fig. 2 and it may be seen that the actual $11u\to11l$ inelastic cross

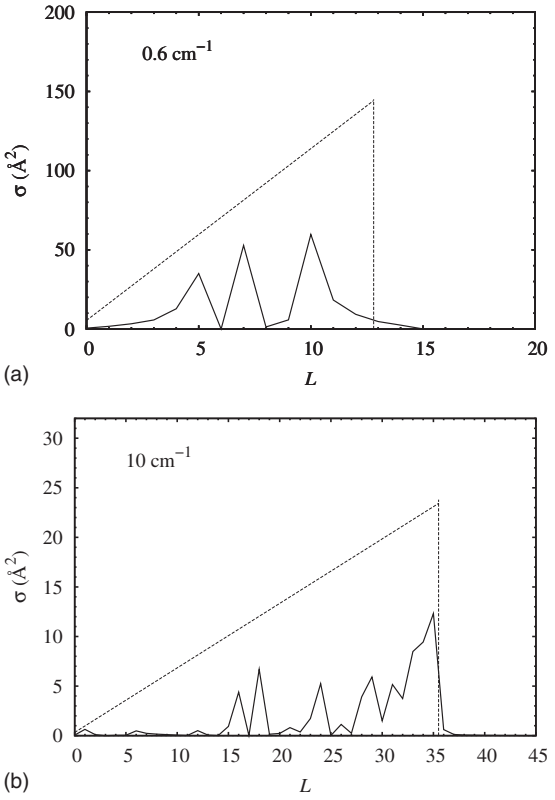

FIG. 3. Partial-wave contributions to inelastic $11u \rightarrow 11l$ cross sections for Rb-ND_3 at collision energies of 0.6 cm^{-1} (upper panel) and 10 cm^{-1} (lower panel). The straight dashed lines show the result corresponding to Langevin capture theory, with a cutoff determined by the heights of the centrifugal barriers calculated for the full potential.

section is substantially below it. This is surprising in view of the very large anisotropy which directly couples the $11l$ and $11u$ states. Further insight is given by the partial-wave contributions to the $11u \rightarrow 11l$ cross sections, which are shown for collision energies of 0.6 and 10 cm^{-1} in Fig. 3. In this case the capture cross section corresponds to an elastic S-matrix element of zero for every L below a cutoff due to the centrifugal potential. The partial inelastic cross section is far less than the capture value across most of the range of L. This contrasts with the behavior observed in other strongly coupled systems, such as high-energy HF-HF collisions [39], rotationally inelastic collisions in Ar-N_2 at 300 K [40], and barrierless reactions in alkali metal atom+diatom collisions at energies above 1 mK [41–44], where the partial cross sections *are* close to the capture value for all L.

A possible explanation for the low inelasticity for Rb-ND_3 is that, despite the large anisotropy, the collisions are approximately adiabatic in the rotation-inversion coordinates. Figure 4 shows "adiabatic bender" curves for Rb-ND_3, which are eigenvalues of the rotation-inversion Hamiltonian for para-ND_3 at fixed R. It may be seen that the curves correlating with the $11u$ and $11l$ states stay far apart for all values of R, with no avoided crossings between them where strong nonadiabatic transitions would be expected.

The resonances are much stronger in the inelastic cross sections than the elastic cross sections. They are particularly

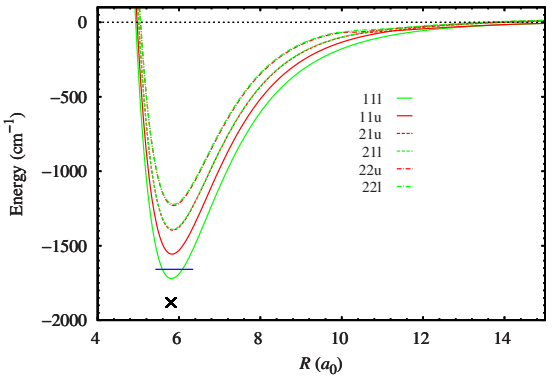

FIG. 4. (Color online) Adiabatic bender curves for Rb interacting with para-ND_3. The line types indicate the level that each curve correlates with at long range and not the character of the adiabatic state at short range. The cross indicates the position of the absolute minimum of the potential surface and the horizontal line indicates the energy of the lowest bound state, −1658.252 cm^{-1}.

strong for collision energies up to about 20 cm^{-1}, as can be seen in the expanded view of the energy dependence of $\sigma_{11u \rightarrow 11l}$ in Fig. 5. For Rb-ND_3 at low energies the resonances can enhance inelastic cross sections by up to a factor of 2. As the collision energy increases the resonances again become weaker and wash out. We see significantly more resonances for Rb-ND_3 than for Rb-NH_3. A detailed description of the origin of the resonances for low kinetic energies will be given in Sec. III B.

The coupled-states approximation is not expected to be accurate at very low energies because it approximates the

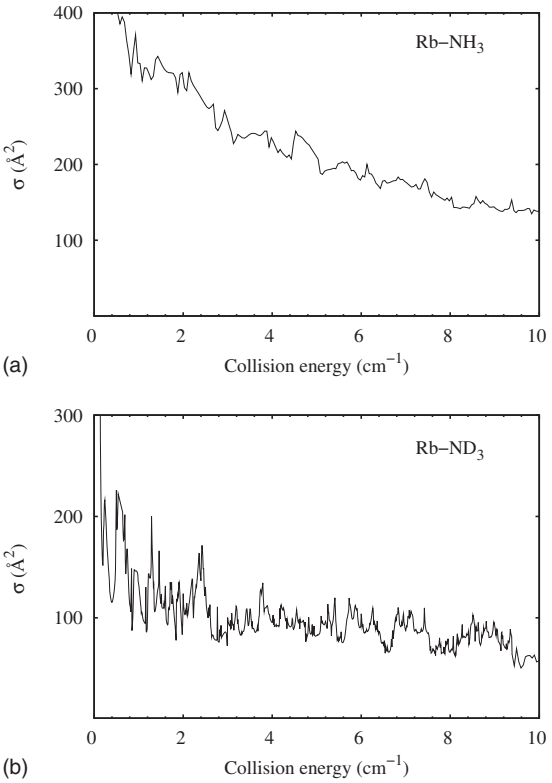

FIG. 5. Resonances in the inelastic $11u \rightarrow 11l$ cross sections for Rb-NH_3 and Rb-ND_3 at low collision energies.

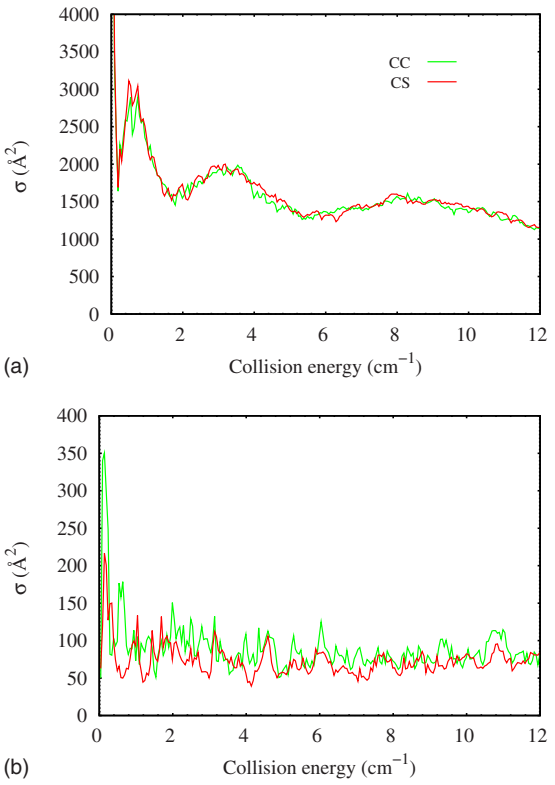

FIG. 6. (Color online) Comparison of elastic $11u \rightarrow 11u$ (upper panel) and inelastic $11u \rightarrow 11l$ (lower panel) cross sections for Rb-ND_3 calculated with CS and CC methods for a restricted basis set with $j_{max}=6$, $k_{max}=5$.

centrifugal terms in the potential and neglects couplings between different helicities. Unfortunately, full close-coupling (CC) calculations for higher energies are prohibitively expensive for partial waves corresponding to large values of J. For example, the basis set used above ($j_{max}=21$ and $k_{max}=8$), which gives 210 channels for para-ND_3 in the CS approximation, produces 2745 channels for each parity in CC calculations for $J \geq 21$. However, it is possible to make the comparison for a restricted basis set, and the results are shown in Fig. 6 for a basis set with $j_{max}=6$, $k_{max}=5$. The terms that are neglected in the CS approximation cause small shifts in resonance positions and intensities, so that it is not possible to make a valid comparison at any individual collision energy. However, the general extent of the resonance structure is similar in the two calculations and the inelastic cross sections typically agree within 5% above 30 cm^{-1}. We can therefore have confidence in the general features of the CS calculations for the full basis set.

The state-to-state cross sections from the $11u$ state to other $j=1-3$ states are shown as a function of collision energy in Fig. 7. As the transition to each additional rotational state becomes energetically allowed, the corresponding excitation cross section rises sharply from zero. This behavior could be seen readily in experiments that use state-selective detection for the scattered ND_3. However, since the cross sections for rotational excitation are very small compared to those for $11u \rightarrow 11l$ relaxation at these energies, we do not see any significant changes in the total inelastic cross section as new channels open up.

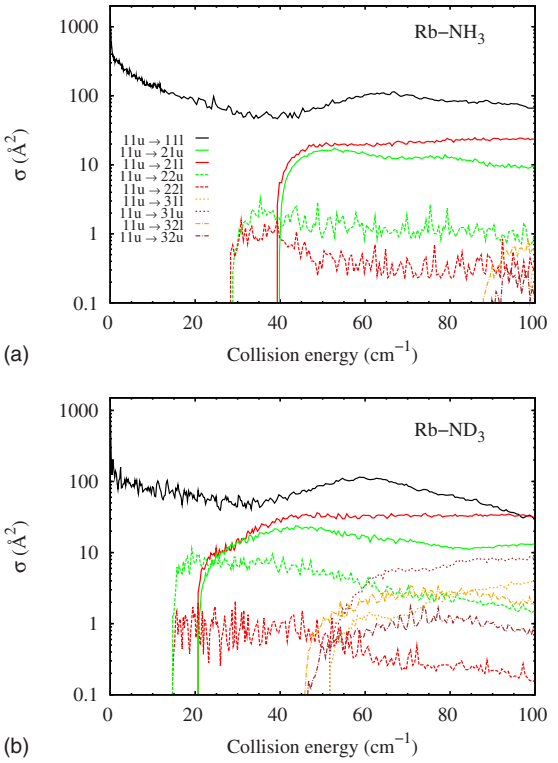

FIG. 7. (Color online) State-to-state inelastic cross sections from the $11u$ state of Rb-NH_3 and Rb-ND_3 as a function of collision energy from coupled-states calculations.

Figure 8 shows the threshold behavior in more detail for the contributions to the cross section $\sigma_{11u \rightarrow 21l}$ obtained from CC calculations for different partial waves J with the full basis set. CC calculations are feasible in this case because only low partial waves contribute just above threshold. At very low energy, each partial-wave contribution follows the Wigner threshold law [45] and is proportional to $(E_{coll} - E_{thresh})^{L_{final}+1/2}$, where E_{coll} and E_{thresh} are the collision energy and the threshold energy, respectively. L takes the lowest allowed value for the threshold level: for $j_{final}=2$, $L=0$ for $J=2$, $L=1$ for $J=1$ and 3, and $L=2$ for $J=0$ and 4. For any final j there is always one total angular momentum (J

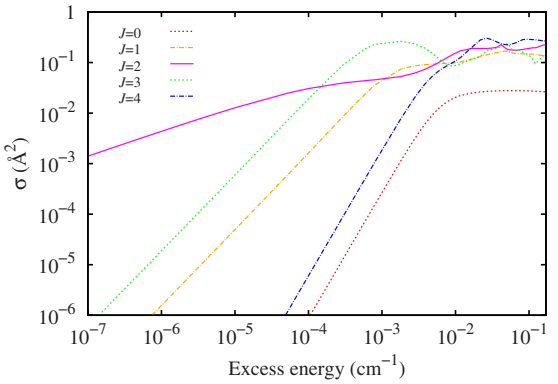

FIG. 8. (Color online) Near-threshold behavior of individual partial-wave contributions to the $11u \rightarrow 21l$ inelastic excitation cross section, from close-coupling calculations, as a function of the excess energy above the threshold for excitation.

$=j$) and parity combination that allows $L=0$ in the outgoing channel, and this dominates the integral cross section for excess energies below 10^{-4} cm^{-1}. Above this, however, additional partial waves contribute and simple $(E_{\mathrm{coll}}-E_{\mathrm{thresh}})^{1/2}$ behavior is not expected for the integral cross section.

For Rb-NH_3, the $11u \rightarrow 11l$ transition is much stronger than any other inelastic transition for the whole range of collision energies considered here. For Rb-ND_3, $\sigma_{11u\rightarrow 21l}$ becomes comparable to $\sigma_{11u\rightarrow 11l}$ for kinetic energies around 100 cm^{-1}. The resonances in individual state-to-state cross sections are in some cases quite strong compared to their backgrounds, especially closely above the thresholds. However, since their magnitude is much smaller than $\sigma_{11u\rightarrow 11l}$, these resonances are not visible in the total inelastic cross section.

There are clear propensity rules that apply to the cross sections, as observed previously for He-NH_3 [23–25,46] and Ar-NH_3 [26,47] collisions. The general effect has been discussed by Alexander [48]. For k-conserving collisions, inversion-changing transitions are preferred when Δj is odd and inversion-conserving transitions are preferred when Δj is even. Thus $\sigma_{11u\rightarrow 21l}$ is larger than $\sigma_{11u\rightarrow 21u}$ since the $11u$ and $21l$ channels are directly coupled by V_{10} potential term. Conversely, for collisions with $\Delta k=1$, which are driven by the V_{33} potential term, inversion-conserving transitions are preferred when Δj is odd, whereas inversion-changing transitions are preferred when Δj is even. Thus $\sigma_{11u\rightarrow 22u}$ is much larger than $\sigma_{11u\rightarrow 22l}$. It is interesting that these propensity rules survive in a system as strongly coupled as Rb-NH_3.

B. Analysis of scattering resonances

There are in principle two types of resonance that might be seen in low-energy collisions. Shape resonances correspond to quasibound states that are confined behind a centrifugal barrier, whereas Feshbach resonances correspond to quasibound states that reside principally in channels corresponding to internally excited states. The height of the centrifugal barrier for each L is given approximately by [44]

$$V_{\mathrm{max}}^{L}=\left[\frac{\hbar^2 L(L+1)}{\mu}\right]^{3/2}(54C_6)^{-1/2}. \tag{14}$$

This function is compared with the actual barrier heights obtained from the adiabatic bender curves for Rb-ND_3 in Fig. 9; it may be seen that the long-range formula (14) is accurate for low L but overestimates the barrier height by about 10% by $L=30$. However, since Rb-ND_3 has a strongly attractive long-range potential ($C_{60}=523E_h a_0^6$) and large reduced mass, the heights of the centrifugal barriers are much smaller than in lighter systems. As will be seen below, most of the resonances observed in the present work are Feshbach resonances.

The origin of the resonances can be understood if we study the contribution to the inelastic cross sections from individual terms in the partial-wave expansion. The top two panels of Fig. 10 show the $11u \rightarrow 11l$ partial cross sections for $L=0-6$ and $L=7-11$ for Rb-ND_3 collision energies up to 2 cm^{-1}, where there are very strong resonances. The bottom panel shows the S-matrix eigenphase sums [49] for $L=7-11$, which show a sharp rise through π as the energy passes through a resonance.

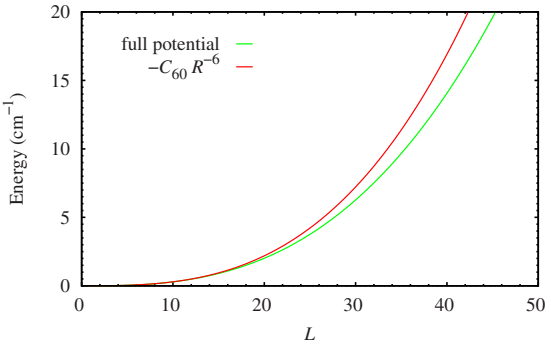

FIG. 9. (Color online) Heights of the centrifugal barrier as a function of L predicted by long-range formula (14) and obtained from the full potential.

In general each partial inelastic cross section shows a nonresonant peak near the corresponding barrier maximum and then dies off at higher energies. The nonresonant peak is quite sharp for low L but broadens as L increases. In particular, the peaks below $E_{\mathrm{coll}}=0.1$ cm^{-1} for $L<6$ are nonresonant. Superimposed on the nonresonant background are peaks and troughs due to resonances. Below the barrier maximum, both shape and Feshbach resonances may occur; however peaks due to Feshbach resonances are suppressed when they are below barriers and it is usually shape resonances that give large peaks in this region.

Above the barrier maximum for each L, Langevin capture theory would predict a partial inelastic cross section,

$$\sigma_{\mathrm{inel}}^{\mathrm{capture}}(L)=\frac{\hbar^2\pi L(L+1)}{2\mu E_{\mathrm{coll}}}. \tag{15}$$

Except at resonances and occasionally near the barrier maximum, the partial cross sections are generally much smaller than this. It is thus evident that low-energy inelastic scattering in Rb-ND_3 is *dominated* by resonant effects.

We also carried out bound-state calculations close to the $j=1$, $k=1$ thresholds to help identify the states responsible for the resonances. The bound-state calculations used the coupled-states approximation with the same basis set as for the collision calculations. The helicity was restricted to $K=1$ since this is the only value that contributes to the $11u \rightarrow 11l$ cross section. The resulting bound states are shown in Fig. 11. Since the rotational energy of the bound and quasibound states of the Rb-ND_3 complex is approximately proportional to $L(L+1)$, it is convenient to plot the energies as a function of this quantity. This allows rotational progressions to be identified as nearly straight lines, and rotational constants can be extracted from the slopes of the lines. However, if there are two or more bound states for the same L with energies very close together, they can mix and avoid one another; an example of this is shown by the dotted lines in Fig. 11.

Most of the peaks in Fig. 10 can be identified with series of bound states. For example, the cross sections for $L=11$

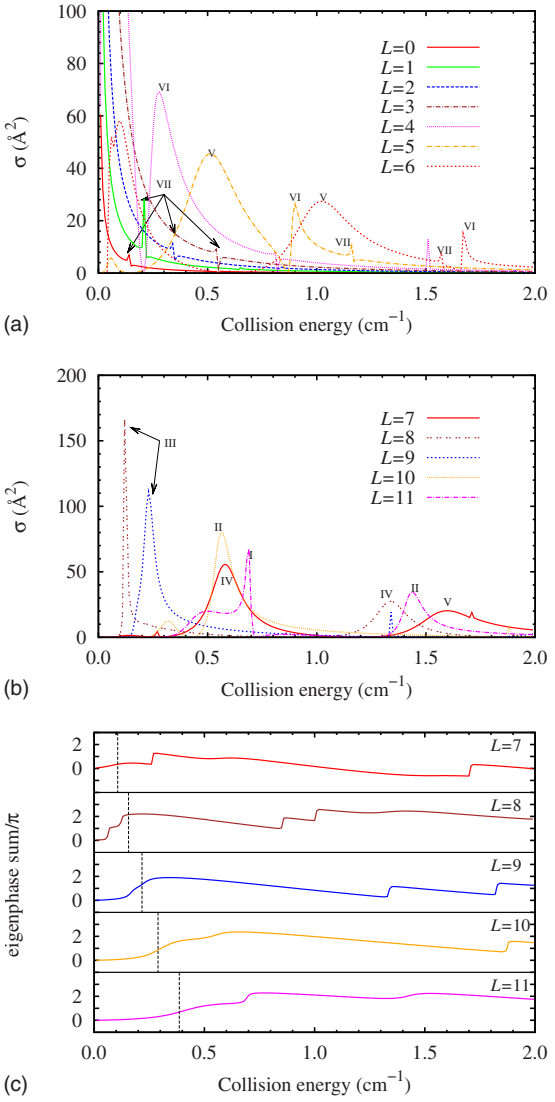

FIG. 10. (Color online) Contributions from partial waves $L=0-6$ (top panel) and $L=7-11$ (center panel) to the inelastic $11u \rightarrow 11l$ cross section for Rb-ND_3. The resonances are labeled by Roman numerals corresponding to the series of bound states shown in Fig. 11. The bottom panel shows eigenphase sums for $L=7-11$. The dashed vertical lines in the bottom panel indicate the positions of centrifugal barriers.

shows three strong peaks. The first of these, at about 0.5 cm^{-1}, is a nonresonant peak associated with the barrier maximum. At higher energies are two resonant peaks, labeled as I and II in Fig. 10. They are associated with characteristic features in the eigenphase sum and can be identified as Feshbach resonances associated with the series of bound states along the dashed lines I and II in Fig. 11; series II also explains the strong peak in the cross section for $L=10$ near 0.6 cm^{-1}. Lines I and II both have a large slope, corresponding to a rotational constant $B \approx 0.04$ cm^{-1} and an effective distance between Rb and ND_3 around $R=9a_0$. It is also not difficult to assign the resonances labeled by IV–VII to the appropriate series of bound states; all these are Feshbach resonances that arise from bound states with small effective intermolecular distances $R<10a_0$. For all these bound states,

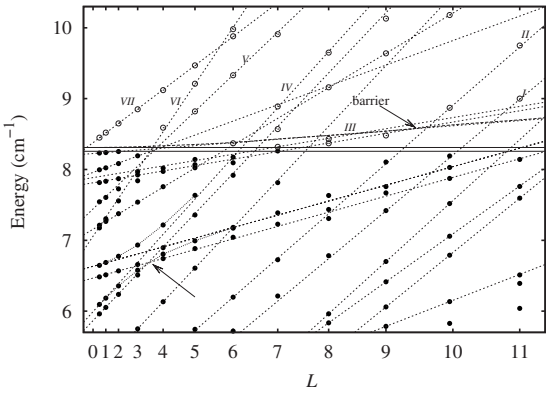

FIG. 11. Near-threshold bound states of Rb-ND_3 (full circles) for helicity $K=1$ as a function of $L(L+1)$. Open circles indicate the positions of the strongest resonances in Fig. 10. The arrow points out an example of an avoided crossing between bound states. The horizontal solid lines at 8.257 and 8.310 cm^{-1} show the $11l$ and $11u$ thresholds, respectively. The dashed line shows the position of centrifugal barrier.

inspection of the wave function near $9a_0$ confirms that they are dominated by rotationally excited basis functions with $j>1$.

The levels along line III in Fig. 11, which give strong resonances for $L=8$ and 9, are associated with quasibound states of significantly smaller rotational constant, $B \approx 0.008$ cm^{-1}, and an effective intermolecular distance around $20a_0$. The dominant contributions to the wave function in this case are the two $j=1$, $k=1$ states; the u and l states contribute almost equally and with opposite signs, corresponding to a single umbrella state of noninverting ND_3. This suggests that these are shape resonances, and indeed for $L=8$ and 9 they lie below the energy of the centrifugal barrier, shown as a dashed curve in Fig. 11. For $L>9$ the extrapolated energy of line III is above the barrier maximum and no well-defined shape resonances occur.

It is important to appreciate that the absolute energies of the resonances and bound states close to threshold are strongly dependent on the potential energy surface. Thus, the studies reported in this section should be treated as a paradigm for understanding the resonant behavior of cross sections rather than as predictions of the actual energies at which resonances will appear for Rb-ND_3.

C. Prospects for sympathetic cooling

As described in Sec. I, there is great interest in the possibility of sympathetic cooling, in which molecules are cooled by thermal contact with a gas of laser-cooled atoms such as Rb. The simplest sympathetic cooling experiment would overlap an electrostatic trap containing a sample of cold molecules such as ND_3 with a gas of atoms in a magnetic or magneto-optical trap. It is therefore of considerable interest to explore collision cross sections for promising candidate atoms and molecules in the temperature regime between 1 μK and 100 mK.

An electrostatic trap works only for molecules in low-field-seeking states, and for NH_3 and ND_3 the low-field-

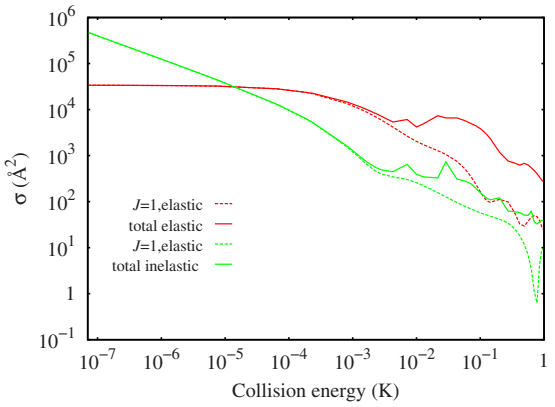

FIG. 12. (Color online) Ultracold limit of the elastic $11u \rightarrow 11u$ and inelastic $11u \rightarrow 11l$ cross sections and the contribution from s-wave scattering ($J=1$) from close-coupling calculations.

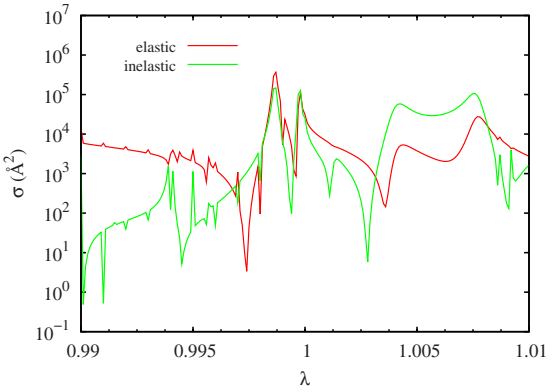

FIG. 13. (Color online) Sensitivity of the elastic $11u \rightarrow 11u$ and inelastic $11u \rightarrow 11l$ cross sections for Rb-ND_3 at a collision energy of 10 μK to a scaling factor λ applied to the interaction potential.

seeking states correlate at low field with the upper state of the tunneling doublet. It is thus very important to know whether collisions with ultracold Rb will cause relaxation to the lower tunneling state, which is a high-field-seeking state and cannot be trapped electrostatically. More specifically, we need to know whether the cross section for the relaxation from $11u$ to $11u$ state is sufficiently small compared to the elastic cross section.

To explore this we have performed close-coupling calculations for very low energies using the same rotational basis set as for the CS calculations described above. In Fig. 12 we show the elastic and total inelastic integral cross sections calculated for partial waves $J=0-8$, which give reasonable convergence for collision energies up to 100 mK. The contribution to the total cross sections from s-wave scattering ($J=1$ partial wave) is dominant in the microkelvin regime. The Wigner threshold behavior for s-wave scattering is followed for kinetic energies up to about 100 μK. Elastic cross sections are larger than inelastic cross sections for collision energies above 100 μK, but never by much more than a factor of 10. For sympathetic cooling, the commonly stated rule of thumb is that the ratio of elastic-to-inelastic cross sections should be at least 100. Thus it appears that the inelastic cross sections are too large to allow ND_3 molecules in low-field-seeking states to be cooled to submillikelvin temperatures by collision with ultracold Rb atoms.

There remains the possibility of using sympathetic cooling for molecules in high-field-seeking states, which can be confined using an alternating current trap [50,51]. Confinement of Rb atoms in such a trap has also been demonstrated [52], but the ac frequencies required are quite different in the two cases. It is therefore important to know whether sympathetic cooling of ND_3 molecules in high-field-seeking states might be feasible using magnetically trapped Rb atoms, which are themselves in low-field-seeking states that are not the ground state in the applied magnetic field. In previous work on Rb-OH collisions [19,53], we found large cross sections for low-energy collisions that changed the hyperfine state of Rb. We initially anticipated [20] that this would occur for Rb-ND_3 collisions as well. However, the more thorough analysis of the collision Hamiltonian in Sec. II B above suggests that for molecules in closed-shell singlet states the atomic spins are likely to be almost unaffected by collisions. We therefore now consider that sympathetic cooling of high-field-seeking states of ND_3 (or NH_3) by magnetically trapped Rb (or another laser-cooled atomic gas) has a good prospect of success.

D. Sensitivity to the interaction potential

Collision calculations at ultralow kinetic energies are very sensitive to details of the potential used in the calculations. Quantitative theoretical predictions of parameters related to scattering cross sections, such as the highest bound states or scattering lengths, are possible only for the simplest lightest systems such as metastable helium [54,55] or hydrogen-lithium mixtures [56]. The calculated Rb-NH_3 interaction potential we use in this paper suffers from many uncertainties resulting from incompleteness of the electronic basis set, the approximate treatment of electronic correlation, relativistic effects, etc., which limit its accuracy to at best a few percent.

To explore this sensitivity, we introduce an additional scaling factor λ into the definition of the interaction potential. We varied the scaling factor between 0.90 and 1.05 and shown the variation in the s-wave elastic $\sigma_{11u\rightarrow 11u}$ and inelastic $\sigma_{11u\rightarrow 11l}$ cross sections (using close-coupling calculations) for a collision energy of 10 μK. The results for a representative slice of the range of λ studied are shown in Fig. 13. The elastic and inelastic cross sections vary dramatically as bound states cross threshold and appear as scattering resonances. In the range of λ explored, the elastic and inelastic cross sections pass through more than ten resonances. There are some values of λ, such as near $\lambda=0.99$, where the inelastic cross section $\sigma_{11u\rightarrow 11l}$ is significantly suppressed by the presence of a strong resonance, but for most other values of the scaling parameter the elastic-to-inelastic ratio ranges lies between 10 and 0.1. Although it is possible that the real potential might produce inelastic cross sections low enough to allow sympathetic cooling for low-field-seeking states, it is quite unlikely.

IV. CONCLUSIONS

We have studied collisions between Rb atoms and NH_3/ND_3 molecules, motivated by recent progress [9,10] in

collision experiments involving velocity-controlled and Stark-decelerated beams of molecules and by interest in the possibility of sympathetic cooling. We focused principally on NH_3 or ND_3 molecules initially in the upper component of the inversion doublet for $j=1$, $k=1$. This level correlates with the low-field-seeking state in an electric field, which can be slowed by Stark deceleration and trapped in an electrostatic trap. We considered collision energies between 0 and 100 cm^{-1}. Using the coupled-states approximation, we calculated the elastic cross sections and state-to-state inelastic cross sections from the low-field-seeking $j=1$, $k=1$ state to other rotation-inversion levels.

The inelastic cross sections are smaller than expected for such a strongly coupled system but are still only about a factor of 10 smaller than the elastic cross section over most of the energy range considered. Both the elastic and inelastic cross sections show dense structure due to scattering resonances. The resonances in the elastic cross sections are diffuse and rather weak compared to the background. The total inelastic cross sections have much stronger resonances compared to their background, especially at collision energies below about 20 cm^{-1}, and one can consider the inelastic scattering as *mostly* resonant in nature. These resonances are washed out for larger collision energies. For energies below 90 cm^{-1} the $11u \rightarrow 11l$ inelastic cross section makes the largest contribution to the total inelastic cross section. Transitions to $j=2$ and 3 do not change the total inelastic cross section significantly as the new channels become energetically accessible at higher collision energies.

We have considered the origin of the scattering resonances using calculations of the bound states of Rb-ND_3 near threshold. Since the long-range attraction between Rb and ND_3 is very strong and the reduced mass is fairly large, the resulting centrifugal barriers are much smaller than in lighter systems. Most of the resonances appearing in the cross sections arise from quasibound states in which Rb interacts with rotationally excited ND_3 and can be classified as Feshbach resonances.

Finally we studied the ultracold limit of the elastic and inelastic cross sections in order to test whether low-field-seeking molecules could be cooled to microkelvin temperatures by contact with an ultracold gas of Rb atoms. Hyperfine effects were neglected. We found that inelastic collisions are strong, and the elastic-to-inelastic ratio is unlikely to be sufficient to achieve sympathetic cooling of ND_3 molecules in the $11u$ state. However, there is a good prospect that sympathetic cooling will be possible for high-field-seeking states of ND_3 or NH_3 even if the atoms used as a coolant are in low-field-seeking states.

ACKNOWLEDGMENTS

The authors are grateful to Heather Lewandowski for sparking their interest in Rb-NH_3 collisions and to Ruth LeSueur for discussions on the effect of the ammonia inversion on the collisions. The authors are grateful to EPSRC for funding of the collaborative project CoPoMol under the ESF EUROCORES program EuroQUAM.

[1] J. D. Weinstein, R. deCarvalho, T. Guillet, B. Friedrich, and J. M. Doyle, Nature (London) **395**, 921 (1998).
[2] D. Egorov, W. C. Campbell, B. Friedrich, S. E. Maxwell, E. Tsikata, L. D. van Buuren, and J. M. Doyle, Eur. Phys. J. D **31**, 307 (2004).
[3] H. L. Bethlem and G. Meijer, Int. Rev. Phys. Chem. **22**, 73 (2003).
[4] H. L. Bethlem, M. R. Tarbutt, J. Küpper, D. Carty, K. Wohlfart, E. A. Hinds, and G. Meijer, J. Phys. B **39**, R263 (2006).
[5] T. Junglen, T. Rieger, S. A. Rangwala, P. W. H. Pinkse, and G. Rempe, Eur. Phys. J. D **31**, 365 (2004).
[6] R. Fulton, A. I. Bishop, M. N. Shneider, and P. F. Barker, Nat. Phys. **2**, 465 (2006).
[7] M. S. Elioff, J. J. Valentini, and D. W. Chandler, Science **302**, 1940 (2003).
[8] C. E. Heiner, H. L. Bethlem, and G. Meijer, Phys. Chem. Chem. Phys. **8**, 2666 (2006).
[9] J. J. Gilijamse, S. Hoekstra, S. Y. T. van de Meerakker, G. C. Groenenboom, and G. Meijer, Science **313**, 1617 (2006).
[10] B. C. Sawyer, B. K. Stuhl, D. Wang, M. Yeo, and J. Ye, Phys. Rev. Lett. **101**, 203203 (2008).
[11] R. D. Levine, B. R. Johnson, J. T. Muckerman, and R. B. Bernstein, Chem. Phys. Lett. **1**, 517 (1968).
[12] F. Fernandez-Alonso and R. N. Zare, Annu. Rev. Phys. Chem. **53**, 67 (2002).
[13] K. Liu, R. T. Skodje, and D. E. Manolopoulos, PhysChemComm **5**, 27 (2002).
[14] J. M. Hutson and F. R. McCourt, J. Chem. Phys. **80**, 1135 (1984).
[15] N. Balakrishnan, A. Dalgarno, and R. C. Forrey, J. Chem. Phys. **113**, 621 (2000).
[16] H. L. Bethlem, G. Berden, F. M. H. Crompvoets, R. T. Jongma, A. J. A. van Roij, and G. Meijer, Nature (London) **406**, 491 (2000).
[17] H. L. Bethlem, F. M. H. Crompvoets, R. T. Jongma, S. Y. T. van de Meerakker, and G. Meijer, Phys. Rev. A **65**, 053416 (2002).
[18] P. Soldán and J. M. Hutson, Phys. Rev. Lett. **92**, 163202 (2004).
[19] M. Lara, J. L. Bohn, D. Potter, P. Soldán, and J. M. Hutson, Phys. Rev. Lett. **97**, 183201 (2006).
[20] P. S. Żuchowski and J. M. Hutson, Phys. Rev. A **78**, 022701 (2008).
[21] T. S. Ho and H. Rabitz, J. Chem. Phys. **104**, 2584 (1996).
[22] P. Soldán and J. M. Hutson, J. Chem. Phys. **112**, 4415 (2000).
[23] S. Green, J. Chem. Phys. **73**, 2740 (1980).
[24] S. Green, J. Chem. Phys. **64**, 3463 (1976).
[25] S. L. Davis and J. E. Boggs, J. Chem. Phys. **69**, 2355 (1978).
[26] G. C. M. van der Sanden, P. E. S. Wormer, A. van der Avoird, J. Schleipen, and J. J. ter Meulen, J. Chem. Phys. **97**, 6460 (1992).
[27] J. W. I. van Bladel, A. van der Avoird, and P. E. S. Wormer, J.

Phys. Chem. **95**, 5414 (1991).
[28] C. H. Townes and A. L. Schawlow, *Microwave Spectroscopy* (Mc-Graw Hill, New York, 1955).
[29] R. L. Poynter and J. S. Margolis, Mol. Phys. **48**, 401 (1983).
[30] S. Urban, D. Papuněk, M. Bester, K. Yamada, G. Winnewisser, and G. Guamieri, J. Mol. Spectrosc. **106**, 29 (1984).
[31] P. McGuire and D. J. Kouri, J. Chem. Phys. **60**, 2488 (1974).
[32] R. T Pack, J. Chem. Phys. **60**, 633 (1974).
[33] J. M. Hutson and S. Green, MOLSCAT, Version 14, distributed by Collaborative Computational Project No. 6 of the UK Engineering and Physical Sciences Research Council, 1994.
[34] M. H. Alexander and D. E. Manolopoulos, J. Chem. Phys. **86**, 2044 (1987).
[35] D. E. Manolopoulos, J. Chem. Phys. **85**, 6425 (1986).
[36] M. H. Alexander, J. Chem. Phys. **81**, 4510 (1984).
[37] M. S. Child, *Semiclassical Mechanics with Molecular Applications* (Oxford University Press, New York, 1991), p. 212.
[38] R. D. Levine and R. B. Bernstein, *Molecular Reaction Dynamics and Chemical Reactivity* (Oxford University Press, New York, 1987).
[39] M. H. Alexander, J. Chem. Phys. **73**, 5135 (1980).
[40] J. N. L. Connor, H. Sun, and J. M. Hutson, J. Chem. Soc., Faraday Trans. **86**, 1649 (1990).
[41] M. T. Cvitaš, P. Soldán, J. M. Hutson, P. Honvault, and J. M. Launay, Phys. Rev. Lett. **94**, 033201 (2005).
[42] G. Quéméner, P. Honvault, J. M. Launay, P. Soldán, D. E. Potter, and J. M. Hutson, Phys. Rev. A **71**, 032722 (2005).
[43] M. T. Cvitaš, P. Soldán, J. M. Hutson, P. Honvault, and J. M. Launay, J. Chem. Phys. **127**, 074302 (2007).
[44] J. M. Hutson and P. Soldán, Int. Rev. Phys. Chem. **26**, 1 (2007).
[45] E. P. Wigner, Phys. Rev. **73**, 1002 (1948).
[46] T. Oka, J. Chem. Phys. **48**, 4919 (1968).
[47] G. C. M. van der Sanden, P. E. S. Wormer, A. van der Avoird, J. Schleipen, and J. J. ter Meulen, J. Chem. Phys. **103**, 10001 (1995).
[48] M. H. Alexander, J. Chem. Phys. **77**, 1855 (1982).
[49] C. J. Ashton, M. S. Child, and J. M. Hutson, J. Chem. Phys. **78**, 4025 (1983).
[50] J. van Veldhoven, H. L. Bethlem, and G. Meijer, Phys. Rev. Lett. **94**, 083001 (2005).
[51] H. L. Bethlem, J. van Veldhoven, M. Schnell, and G. Meijer, Phys. Rev. A **74**, 063403 (2006).
[52] S. Schlunk, A. Marian, P. Geng, A. P. Mosk, G. Meijer, and W. Schöllkopf, Phys. Rev. Lett. **98**, 223002 (2007).
[53] M. Lara, J. L. Bohn, D. E. Potter, P. Soldán, and J. M. Hutson, Phys. Rev. A **75**, 012704 (2007).
[54] M. Przybytek and B. Jeziorski, J. Chem. Phys. **123**, 134315 (2005).
[55] A. S. Dickinson, F. X. Gadea, and T. Leininger, J. Phys. B **37**, 587 (2004).
[56] F. X. Gadea, T. Leininger, and A. S. Dickinson, Eur. Phys. J. D **15**, 251 (2001).